Article

Cell

Pumilio1 Haploinsufficiency Leads to SCA1-like Neurodegeneration by Increasing Wild-Type Ataxin1 Levels

Graphical Abstract

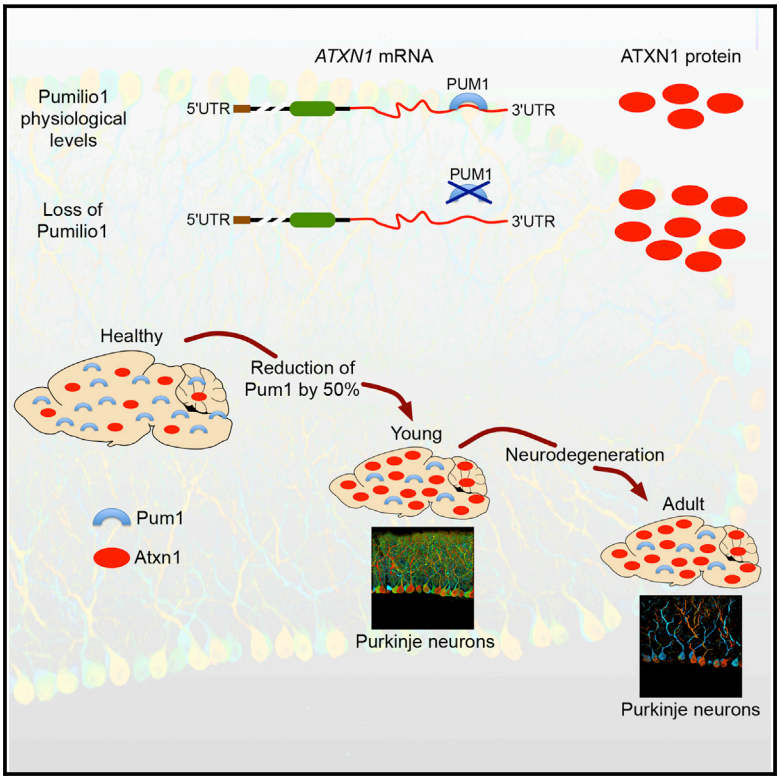

Highlights

- The RNA-binding protein PUMILIO1 regulates levels of ATAXIN1 protein and mRNA
- A modest increase in wild-type Ataxin1 levels is enough to cause neurodegeneration
- *Pumilio1* haploinsufficiency accelerates SCA1 disease progression
- *Ataxin1* haploinsufficiency rescues *Pumilio1*$^{+/-}$ phenotypes

Authors

Vincenzo A. Gennarino, Ravi K. Singh, ..., Roy V. Sillitoe, Huda Y. Zoghbi

Correspondence

hzoghbi@bcm.edu

In Brief

Pumilio1 is an RNA-binding protein that binds *Ataxin1* mRNA and regulates its stability. Haploinsufficiency of *Pumilio1* results in an increase in Ataxin1 levels, leading to progressive motor dysfunction and degeneration of Purkinje cells, features typical of spinocerebellar ataxia type 1. These data suggest that either haploinsufficiency of *PUMILIO1* or duplication of *ATAXIN1* could contribute to neurodegeneration in humans.

Gennarino et al., 2015, Cell *160*, 1087–1098
March 12, 2015
http://dx.doi.org/10.1016/j.cell.2015.02.012

CellPress

Article

Cell

Pumilio1 Haploinsufficiency Leads to SCA1-like Neurodegeneration by Increasing Wild-Type Ataxin1 Levels

Vincenzo A. Gennarino,[1,10] Ravi K. Singh,[2] Joshua J. White,[2,3,10] Antonia De Maio,[4,10] Kihoon Han,[1,5,10] Ji-Yoen Kim,[1,10] Paymaan Jafar-Nejad,[1,10,12] Alberto di Ronza,[1,10] Hyojin Kang,[1,10,13] Layal S. Sayegh,[1,10,14] Thomas A. Cooper,[2,4,6,7,8] Harry T. Orr,[11] Roy V. Sillitoe,[2,3,4,10] and Huda Y. Zoghbi[1,2,4,5,9,10,*]

[1]Department of Molecular and Human Genetics
[2]Department of Pathology and Immunology
[3]Department of Neuroscience
[4]Program in Developmental Biology
[5]Howard Hughes Medical Institute
[6]Department of Molecular and Cellular Biology
[7]Dan L. Duncan Cancer Center
[8]Department of Molecular Physiology and Biophysics
[9]Department of Pediatrics
Baylor College of Medicine, Houston, TX 77030, USA
[10]Jan and Dan Duncan Neurological Research Institute at Texas Children's Hospital, Houston, TX 77030, USA
[11]Institute for Translational Neuroscience, Department of Laboratory Medicine and Pathology, University of Minnesota, Minneapolis, MN 55455, USA
[12]Present address: Isis Pharmaceuticals, Inc. 2855 Gazelle Court, Carlsbad, CA 92010, USA
[13]Present address: HPC-enabled Convergence Technology Research Division, Korea Institute of Science and Technology Information, Daejeon, South Korea
[14]Present address: Emory University School of Medicine, Atlanta, GA 30322, USA
*Correspondence: hzoghbi@bcm.edu
http://dx.doi.org/10.1016/j.cell.2015.02.012

SUMMARY

Spinocerebellar ataxia type 1 (SCA1) is a paradigmatic neurodegenerative proteinopathy, in which a mutant protein (in this case, ATAXIN1) accumulates in neurons and exerts toxicity; in SCA1, this process causes progressive deterioration of motor coordination. Seeking to understand how post-translational modification of ATAXIN1 levels influences disease, we discovered that the RNA-binding protein PUMILIO1 (PUM1) not only directly regulates ATAXIN1 but also plays an unexpectedly important role in neuronal function. Loss of *Pum1* caused progressive motor dysfunction and SCA1-like neurodegeneration with motor impairment, primarily by increasing Ataxin1 levels. Breeding $Pum1^{+/-}$ mice to SCA1 mice ($Atxn1^{154Q/+}$) exacerbated disease progression, whereas breeding them to $Atxn1^{+/-}$ mice normalized Ataxin1 levels and largely rescued the $Pum1^{+/-}$ phenotype. Thus, both increased wild-type ATAXIN1 levels and *PUM1* haploinsufficiency could contribute to human neurodegeneration. These results demonstrate the importance of studying post-transcriptional regulation of disease-driving proteins to reveal factors underlying neurodegenerative disease.

INTRODUCTION

Misfolded proteins underlie the pathogenesis of a number of neurodegenerative conditions, collectively known as proteinopathies. Alzheimer disease (AD), Parkinson disease (PD), amyotrophic lateral sclerosis (ALS), and polyglutamine diseases such as Huntington disease all fall into this category (Ross and Poirier, 2004; Soto, 2003). Despite the heterogeneity of their pathogenic mechanisms, in each of these diseases, the misfolded protein accumulates in neurons and exerts toxicity. Somewhat surprisingly, the brain can also be sensitive to elevated levels of wild-type (WT) protein: duplication of the *amyloid precursor protein* (*APP*) locus causes autosomal dominant early-onset AD (Rovelet-Lecrux et al., 2006; Rumble et al., 1989), and duplications or triplications of α-*synuclein* (*SNCA*) are associated with familial PD (Chartier-Harlin et al., 2004; Ibáñez et al., 2004; Singleton et al., 2003). Along similar lines, it has been shown recently that *leucine-rich repeat kinase 2* (*LRRK2*) mutations, the most common cause of inherited PD, increase overall protein synthesis in *Drosophila*, and that reduction in dLRRK levels is protective (Martin et al., 2014).

Spinocerebellar ataxia type 1 (SCA1) is paradigmatic of the subgroup of polyglutamine (polyQ) proteinopathies caused by expansion of an unstable CAG repeat in the coding region of the relevant disease gene, in this case *ATAXIN1* (*ATXN1*) (Orr et al., 1993). The onset of SCA1 is usually in mid-life, when motor coordination begins to deteriorate because of cerebellar degeneration; patients eventually die of bulbar dysfunction that

renders them unable to clear their airway (Zoghbi and Orr, 2009). There is clear evidence that the expanded polyQ tract stabilizes ATXN1 and causes it to resist being cleared by the ubiquitin-proteasome pathway, in effect increasing its abundance in neurons (Cummings et al., 1999). Notably, the severity of neurodegeneration in fly and mouse models of SCA1 correlates directly with levels of mutant ATXN1 protein (Burright et al., 1995; Fernandez-Funez et al., 2000), and massive overexpression of even WT ATXN1 under the Purkinje-cell-specific promoter can produce a mild SCA1-like phenotype in mice (Fernandez-Funez et al., 2000).

Although the artificiality of transgenic models limits their relevance to the human disease, these results from SCA1 transgenic mice, along with the evidence from familial AD and PD patients, led us to ask whether there were post-transcriptional modifications that might increase the levels of WT ATXN1 in a more physiologically relevant way and shed further light on the role of protein levels in neurodegeneration. The extraordinarily long 3′ UTR, approximately 7 kb in *ATXN1* mRNA, seemed to promise a rich source of key brain-enriched post-transcriptional regulatory elements. To our surprise, we found that ATXN1 is regulated directly by an RNA-binding protein (RBP), *Pumilio1*, and that a brain-wide increase in WT Atxn1 levels of only ~50%, caused by *Pum1* haploinsufficiency, is sufficient to cause marked neurodegeneration in mice.

RESULTS

The RBP PUMILIO1 Regulates ATAXIN1 Levels in Cells

Two types of molecules are known to modulate protein levels by binding to the corresponding mRNA: RBPs and microRNAs (miRNAs). RBPs bind to specific sequence motifs or secondary structures in mRNAs and regulate multiple steps in RNA metabolism, such as splicing, nucleus-cytoplasm transport, and translation (Lukong et al., 2008). On the other hand, miRNAs are small non-coding RNAs that control various developmental and physiological processes by suppressing the expression of their target genes via binding of a short (6–8 nucleotide) complementary seed region in the 3′ UTRs of mRNAs (Bartel, 2009).

We first scanned the ~7 kb-long *ATXN1* 3′ UTR for potential binding sites for miRNAs by using the TargetScan (Friedman et al., 2009), CoMeTa (Gennarino et al., 2012), and HOCTARdb (Gennarino et al., 2011) prediction tools. As expected, scanning identified dozens of potential miRNA-binding sites (data not shown). Because RNA folding mediates miRNA-RNA interactions by masking or exposing specific binding-site sequences, we analyzed the secondary structure of the *ATXN1*-3′ UTR (Wan et al., 2014) to prioritize the best candidate *ATXN1*-modulating miRNAs. This revealed a complicated secondary structure that masks the binding sites for almost all of the putative miRNAs that might target the *ATXN1*-3′ UTR (Figure S1). For miRNAs to act on *ATXN1* mRNA, they would likely require the help of RBPs to unfold such a structure.

Scan analysis of the human *ATXN1*-3′ UTR revealed three putative Pumilio1 (PUM1) binding motifs (Wang et al., 2002) at positions 682, 2812, and 5275 from the beginning of the UTR (Figure 1A). The RBP PUM1 regulates its target genes by inducing a conformational switch in the 3′ UTR that unmasks specific miRNA-binding sites (Kedde et al., 2010; Miles et al., 2012). Interestingly, the motif in position 5275 (Figure 1A, red box) is highly conserved across several species and represents the canonical PUM1-binding motif (5′-UGUAXAUA-3′) (Galgano et al., 2008; Wang et al., 2002). Overexpressing *PUM1* in HEK293T cells reduced *ATXN1* mRNA levels, whereas decreasing *PUM1* by two different RNAi increased *ATXN1* mRNA levels (Figure 1B). In vitro overexpression of *PUM1* consistently decreased the luciferase activity of a reporter construct expressing the full-length *ATXN1*-3′ UTR (Figure 1C). Mutation of each PUM1-binding motif within the *ATXN1*-3′ UTR revealed that only the most conserved site, containing the canonical motif, is functional; when mutated, it abolished the effect of *PUM1* overexpression on luciferase activity (Figure 1D).

Pum1 Is Widely Expressed in Mouse Brain and Regulates *Atxn1* Levels In Vivo

To examine the endogenous expression pattern of *Pum1* in mice, we performed in situ hybridization assays (ISH) and western blot on 3-week-old mouse brain sections. *Pum1* was expressed in all major brain regions in WT mice, almost completely absent in the brain of null mice, and reduced in heterozygous ($Pum1^{+/-}$) brains (Figure S2A). We also confirmed that Pum1 protein is widely expressed in the brain at 5 weeks of age (Figure S2B).

To determine whether Pum1 binds *Atxn1* mRNA in vivo, we performed an RNA cross-linking and immunoprecipitation assay (RNA-Clip) on cerebra and cerebella from 5-week-old WT animals, using *Pum1* knockout mice ($Pum1^{-/-}$) as negative controls (Figure S2C). We found that Pum1 physically interacts with the conserved binding site of the *Atxn1*-3′ UTR in WT mice (Figure 2A). Consistent with the finding that Pum1 negatively regulates Atxn1, *Pum1* heterozygous ($Pum1^{+/-}$) mice showed increased levels of both Atxn1 protein (Figure 2B) and mRNA (Figure 2C)—approximately 30% in the cerebrum and 50% in the cerebellum—and $Pum1^{-/-}$ mice showed even more pronounced increases (Figures 2B and 2C). These data demonstrate that Pum1 directly regulates Atxn1 levels in the mouse brain.

PUM1 Controls ATXN1 Levels by Affecting RNA Stability and not through the miRNA Machinery

Several mRNA subsets contain target sites for both RBPs and miRNAs, and cooperation between these two types of post-transcriptional regulators has been described (Bhattacharyya et al., 2006; Fabian and Sonenberg, 2012; Glorian et al., 2011; Kim et al., 2009; Kundu et al., 2012). This may be particularly relevant for PUM1, as studies have indicated extensive interaction between PUM1 and the miRNA regulatory system (Kedde et al., 2010; Galgano et al., 2008).

To determine whether PUM1 regulates ATXN1 through miRNA by inducing a conformational switch in its 3′ UTR, we overexpressed *PUM1* in HEK293T cells along with miR-101a, a miRNA known to modulate *ATXN1* levels (Lee et al., 2008). These conditions significantly reduced levels of ATXN1 protein (Figures 3A and S3A) and mRNA (Figure S3E), but no more than overexpressing miR-101a or *PUM1* separately. In fact, overexpression

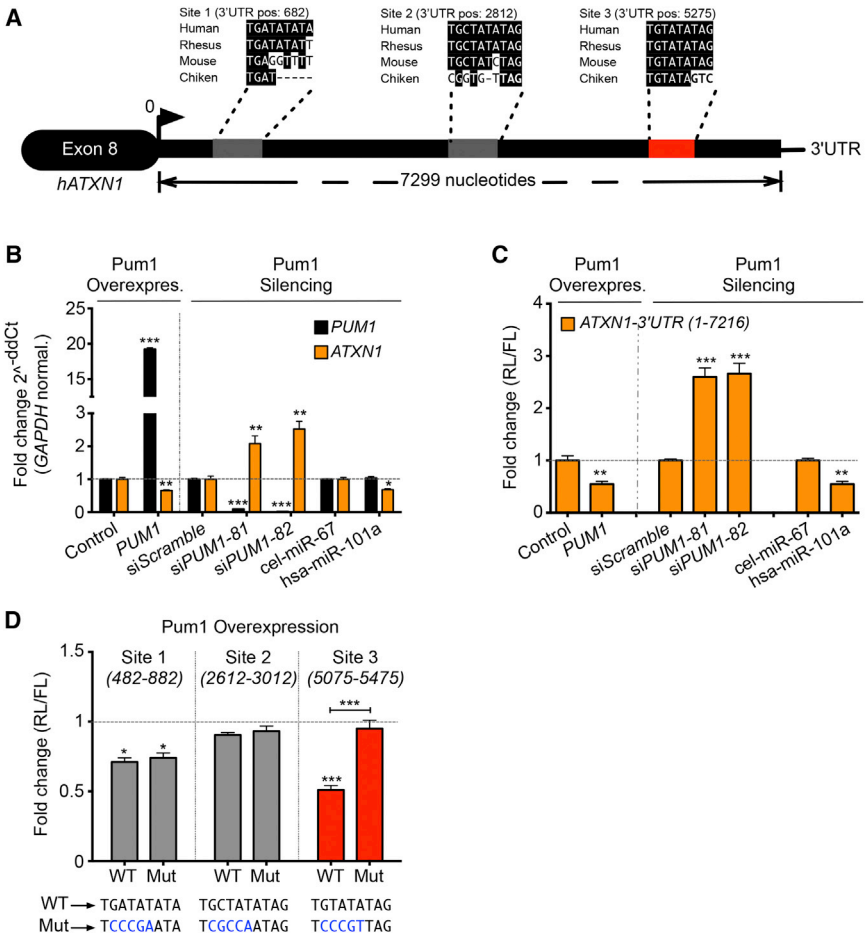

Figure 1. PUM1 Regulates ATXN1 Levels via a Highly Conserved Binding Motif

(A) Schematic representation of human *ATXN1*-3′ UTR showing three putative PUM1-binding motifs (gray and red boxes) and their conservation in different species. The numbers indicate positions of PUM1 motifs in the human *ATXN1*-3′ UTR.

(B) *ATXN1* mRNA quantification by qRT-PCR in HEK293T cells upon overexpression (left panel) or knockdown (si*PUM1*-81 and -82) (right panel) of *PUM1*. The destination-cloning vector (control), scrambled siRNAs (siScr.), and cel-miR-67 were used as negative controls. The housekeeping gene *GAPDH* was used to normalize the expression of genes in all the qRT-PCR experiments.

(C) Luciferase assay in HEK293 cells overexpressing the reporter construct harboring the full-length *ATXN1*-3′ UTR. In these conditions, we overexpressed (left panel) or decreased expression (right panel) of *PUM1*.

(D) Luciferase assay in HEK293T cells transfected with single WT and mutant (MUT) putative PUM1-binding site on the *ATXN1*-3′ UTR. The positions of cloned regions for each PUM1-binding motif are indicated. The mutagenized nucleotides are highlighted in blue.

In (C) and (D), the destination-vector (control), RNAi scramble (siScramble), and cel-miR-67 were used as negative controls; miR-101a was used as positive control. (RL) Renilla, (FL) Firefly luciferase. All the experiments were performed in triplicate (data represent mean ± SEM). p values were calculated by Student's t test. Statistical significance is indicated as follows: *$p < 0.05$, **$p < 0.01$, ***$p < 0.0001$. See also Figure S1.

of miR-101a along with *PUM1* knockdown consistently decreased levels of ATXN1 protein (Figures 3B and S3B) and mRNA (Figure S3F) to a degree comparable to that of miR-101a overexpression alone. These results suggest that PUM1 regulates *ATXN1* in a miR-101a-independent fashion but do not exclude the possibility that other miRNAs bind the ATXN1 3′ UTR. To obviate testing the effect of PUM1 on all possible miRNAs regulating *ATXN1*, we knocked down the catalytic engine of the RNA-induced silencing complex (RISC), *Argonaute-2* (*AGO2),* to globally inhibit miRNA binding and retested PUM1's ability to regulate ATXN1. We found that *PUM1* overexpression in the context of *AGO2* knockdown still reduced levels of both ATXN1 protein (Figures 3C and S3C) and mRNA (Figure S3G). Conversely, simultaneous RNAi of *PUM1* and *AGO2* increased levels of both ATXN1 protein (Figures 3D and S3D) and mRNA (Figure S3H), but no more than silencing *PUM1* alone. These data establish that PUM1 modulates *ATXN1* levels directly by binding its 3′ UTR, without the assistance of the miRNA machinery.

To further explore the mechanism by which PUM1 regulates ATXN1 levels, we tested whether PUM1 influences the stability or the translation of *ATXN1* mRNA. We transfected HEK293T with a luciferase reporter encoding an *ATXN1*-3′ UTR harboring either the conserved WT or mutated (Mut) PUM1-binding site. Later, we used treatment with DRB (5,6-dichloro-1-β-D-ribofuranosylbenzimidazole), a drug that inhibits RNA translation by blocking RNA polymerase II in the early elongation stage, to assess the levels of the reporter transcript. Upon the addition of DRB (time-point zero), the relative expression of reporter transcripts containing the *ATXN1*-3′ UTR Mut binding site is considerably higher than that of transcripts containing the *ATXN1*-3′ UTR WT binding site (Figure 3E, top panel). This difference remains stable over time until 8 hr after DRB addition. Remarkably, the *ATXN1*-3′ UTR with Mut binding site reached its half-life after 19 hr, whereas the *ATXN1*-3′ UTR with WT binding site decreased linearly over time, reaching its half-life at nearly 8 hr (Figure 3E, top panel). Given that the promoter sequences of the *ATXN1*-3′ UTR constructs carrying either WT or Mut binding sites are exactly the same and that transfection of neither construct affected PUM1 protein levels, we conclude that PUM1 promotes degradation of ATXN1 by binding its 3′ UTR (Figures 3E, bottom panel and S3I).

To investigate physiological changes in *ATXN1* mRNA, we decided to knock down *PUM1* in HEK293T cells and measure the half-life of endogenous *ATXN1* mRNA at different time points after DRB treatment. Knockdown of *PUM1* (si*PUM1*) was associated with a significant increase of *ATXN1* mRNA from time zero and remained upregulated up to 8 hr after translation

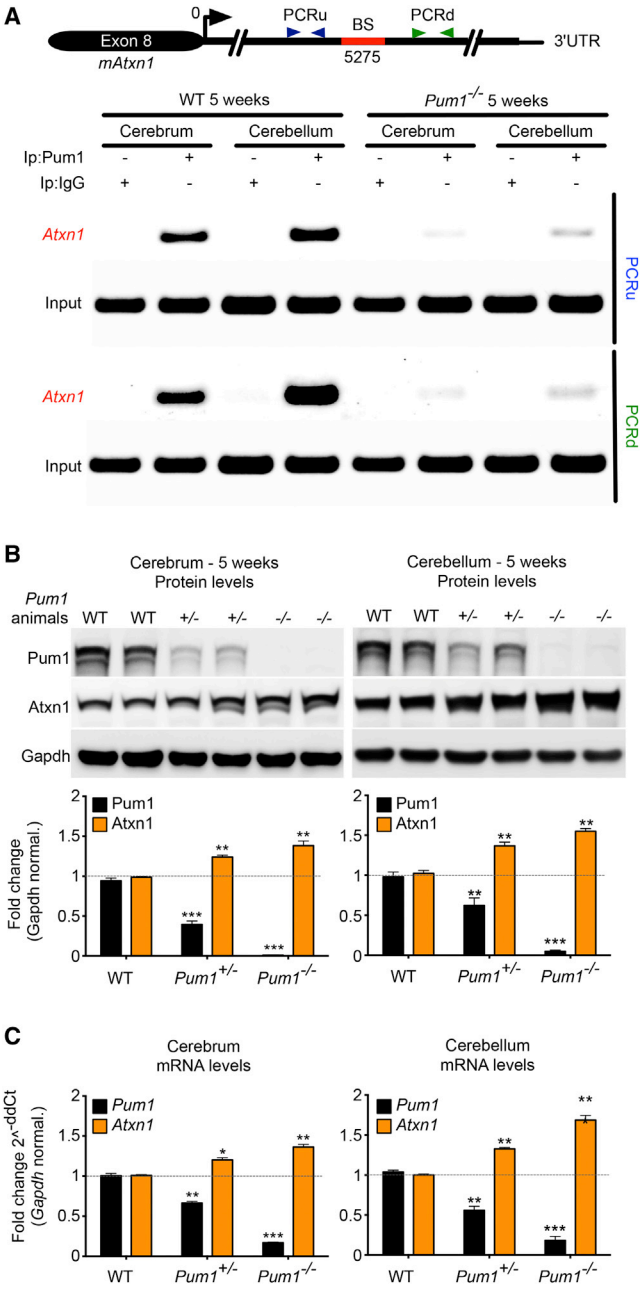

Figure 2. Pum1 Directly Binds the 3′ UTR of *Atxn1* to Regulate Its Levels in Mouse Cerebrum and Cerebellum

(A) RNA-Clip for the conserved Pum1-binding site in mouse cerebrum and cerebellum. PCRu and PCRd highlight the PCR fragments upstream and downstream of the conserved *Atxn1*-3′ UTR Pum1-binding site (BS). IP with IgG as well *Pum1* null mice were used as negative controls. Isolated RNA from a fraction (10%) of pre-cleared lysate was used as input. The experiment was performed in triplicate.

(B and C) Quantification of Atxn1 protein (B) and mRNA levels (C) in WT and $Pum1^{-/-}$ mice in cerebrum and cerebellum (n = 8 per genotype).

Data represent mean ± SEM and normalized to Gapdh. See Experimental Procedures for more details. p values were calculated by Student's t test; *p < 0.05, **p < 0.01, ***p < 0.0001. See also Figure S2.

inhibition (Figure 3F, top panel). Our calculation consistently showed that the half-life of *ATXN1* mRNA was much longer (nearly 12 hr) after si*PUM1* than after siScramble transfection (~4 hr) (Figure 3F, top panel). We confirmed PUM1 downregulation by quantifying mRNA at time zero (Figure S3J) and protein levels at different time points (Figures 3F, bottom panel and S3K). PUM1 thus increases ATXN1 levels by directly regulating the stability of *ATXN1* mRNA.

Pum1 Mutant Mice Develop Progressive Motor Dysfunction and Neurodegeneration

Recent studies have shown that Pum1 is an essential regulator of spermatogenesis in mice and promotes differentiation of embryonic stem cells (Chen et al., 2012; Leeb et al., 2014), but its role in the mammalian nervous system has not been investigated. We therefore characterized the brain structure and behavior of *Pum1* knockout mice (Chen et al., 2012).

The *Pum1* null allele tends to be transmitted with an altered Mendelian ratio (Figure S4A). Compared to WT and $Pum1^{+/-}$ littermates, $Pum1^{-/-}$ mice were significantly smaller in body length, weight, and brain weight and size (Figures 4A and S4B). Surprisingly, the loss of one copy of *Pum1* was sufficient to cause impaired performance on the accelerating rotarod assay in 5-week-old mice (Figure 4B): the motor deficit had progressed in severity by 12 weeks (Figure S4C). This motor incoordination was even more dramatic in $Pum1^{-/-}$ age-matched mice (Figures 4B and S4C), which performed equally poorly in the dowel-walking test (Figures S4D and S4E)—as poorly, in fact, as SCA1 mice at this age in both assays (Watase et al., 2002).

Beginning at 8 weeks of age, both $Pum1^{+/-}$ and $Pum1^{-/-}$ mice exhibited hind-paw clasping when suspended by the tail (Figures 4C and S4F), a sign of neurological dysfunction. At 10 weeks of age, $Pum1^{-/-}$ mice displayed significantly less vertical activity in an open-field chamber (Figure S4G) and spent less time in its center (Figure S4H) but traveled greater distances over 30 min in the chamber than WT (Figure 4D). Interestingly, $Pum1^{-/-}$ mice covered a greater distance at 18 weeks than at 10 weeks of age (Figure S4I). Using the DigiGait assay, we found that 12-week-old $Pum1^{-/-}$ mice had wider stances (Figure S4J), shorter stride lengths (Figure S4K), and greater stride frequencies (Figure S4L). At the same age, $Pum1^{+/-}$ and $Pum1^{-/-}$ mice were poor nest builders (Figure S4M). *Pum1* deficiency thus causes progressive loss of motor coordination that appears to be cerebellar in origin.

To uncover the defects underlying the phenotype, we performed neuropathological studies. At 3 and 4 weeks of age, there was no evidence of Purkinje cell pathology in $Pum1^{+/-}$ or $Pum1^{-/-}$ mice (Figures 4F and S4N), but by 10 weeks, *Pum1* haploinsufficiency had caused loss of Purkinje cells (Figures 4E and 4F) and dendritic arborization (Figure 4G). Both defects were more dramatic in age-matched $Pum1^{-/-}$ mice (Figures 4E–4G). The neuronal loss is thus a result of neurodegeneration and not a developmental defect. Notably, progressive Purkinje cell degeneration and motor dysfunction are hallmarks of SCA1 in both human patients and the SCA1 knockin mouse model ($Atxn1^{154Q/+}$) (Watase et al., 2002). Because the progressive defects in *Pum1* mutant mice were reminiscent of those

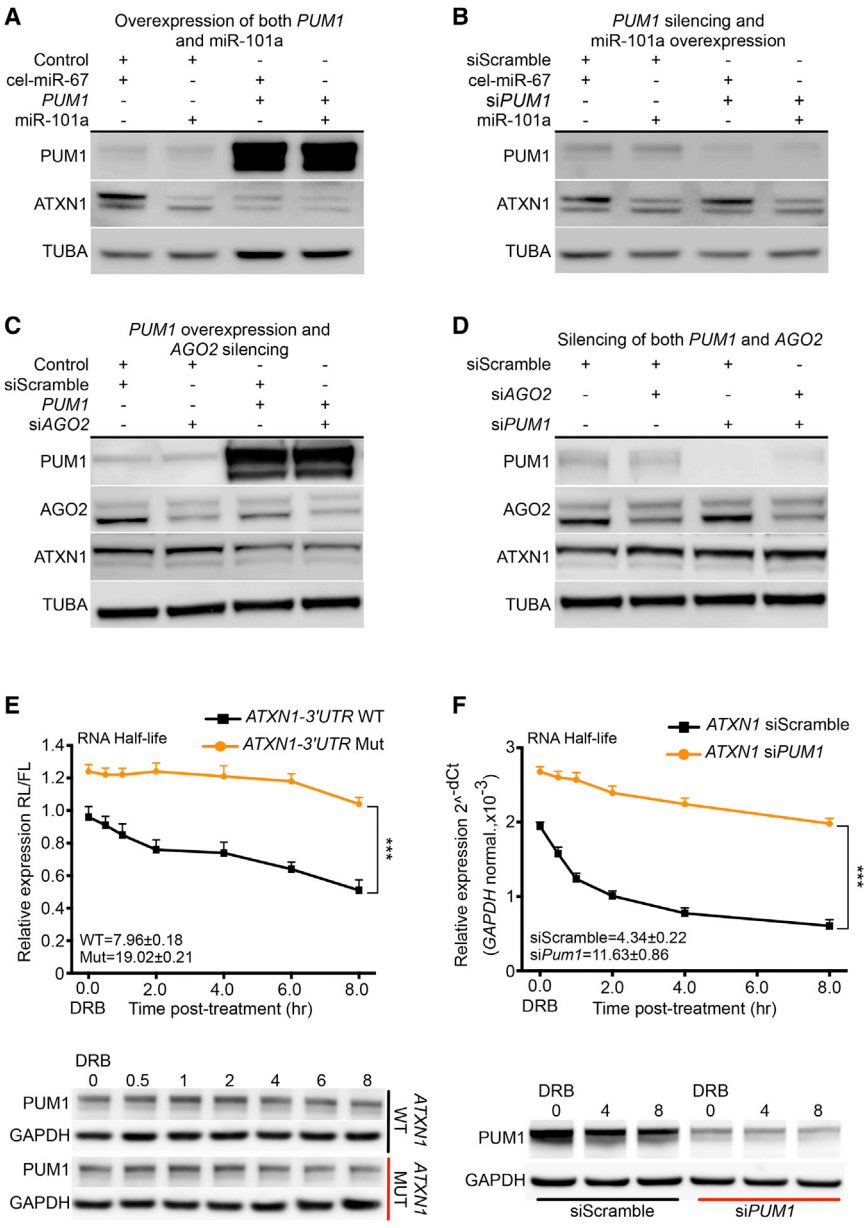

Figure 3. PUM1 Modulates the Levels of WT ATXN1 Independently of miRNAs

(A–D) Representative western blot (upper panel) of protein lysates from HEK293T cells upon (A) overexpression of both *PUM1* and miR-101a; (B) RNAi *PUM1* (si*PUM1*) followed by overexpression of miR-101a; (C) overexpression of *PUM1* followed by RNAi *AGO2* (si*AGO2*); and (D) RNAi of both *PUM1* and *AGO2*. The negative controls were destination-cloning vector (control), RNAi scramble (siScramble), and cel-miR-67. All data were normalized to α-tubulin (TUBA).

(E) mRNA half-life quantification of WT and Mut PUM1 *ATXN1*-3′ UTR binding sites in HEK293T cells at different time points upon DRB treatment (time zero). The numeric values within the panel given the extrapolated half-life for WT and Mut RNA, $p = 3.6 \times 10^{-06}$. Firefly (FL) RNA levels were quantified and normalized to Renilla (RL). Bottom panel: representative western blot of PUM1 in HEK293T cells at different time points. Data were normalized to GAPDH.

(F) *ATXN1* mRNA half-life quantification in HEK293T cells at different time points, from zero (DRB treatment) to 8 hr total upon RNAi of *PUM1* (si*PUM1*) or RNAi of scramble (siScramble) transfection. The numeric values within the panel given the extrapolated half-life for si*PUM1* and siScramble RNA, p = 0.012. Bottom panel: representative western blot of PUM1 in HEK293T cells at different time points.

Data were normalized to *GAPDH* mRNA (top panel) or protein (bottom panel). All experiments were performed in triplicate (data represent mean ± SEM); ***$p < 0.0001$. See also Figure S3.

observed in SCA1 mice (Watase et al., 2002), we decided to dissect the genetic interaction between *Pum1* and SCA1 mice.

Pum1 Haploinsufficiency Worsens the Phenotype of the SCA1 Knockin Mouse

Given that Atxn1 levels were increased in $Pum1^{+/-}$ and in $Pum1^{-/-}$ mice (Figure 2B), we predicted that halving the dosage of *Pum1* in the SCA1 knockin mice ($Pum1^{+/-};Atxn1^{154Q/+}$) would exacerbate the SCA1 phenotype, and this proved to be the case. $Pum1^{+/-};Atxn1^{154Q/+}$ mice tended to be smaller than $Atxn1^{154Q/+}$ and the other genotypes (lower body and brain weights, shorter lengths, smaller brain sizes; Figures S5A and S5B) and showed more severe motor incoordination and hind-paw clasping than either $Atxn1^{154Q/+}$ or $Pum1^{+/-}$ mice (Figures 5A and 5B). Notably, $Pum1^{+/-};Atxn1^{154Q/+}$ mice began to show the hind-paw clasping phenotype at 6 weeks, much earlier than age-matched $Atxn1^{154Q/+}$ mice or *Pum1* single mutants (Figure 5B). At 10 weeks of age, $Pum1^{+/-};Atxn1^{154Q/+}$ mice traveled greater distances than WT and $Atxn1^{154Q/+}$ but not more than $Pum1^{+/-}$ mice (Figure S5C). Severe kyphosis (curvature of the spine) developed in $Pum1^{+/-};Atxn1^{154Q/+}$ mice 8 weeks earlier than SCA1 knockin mice (20 versus 28 weeks; Figure 5C), confirming the accelerated disease course. In addition, $Pum1^{+/-};Atxn1^{154Q/+}$ mice had a significantly shorter lifespan than their $Atxn1^{154Q/+}$ littermates (Figure 5D). At 12 weeks of age, the Purkinje cell loss (Figures 5E and 5F) and arborization defects (Figure 5G) were more dramatic in $Pum1^{+/-};Atxn1^{154Q/+}$ than with all other genotypes. These results suggest a genetic interaction between *Pum1* and $Atxn1^{154Q}$.

Genetic Reduction of Atxn1 Levels Rescued the Pum1 Mutant Phenotype

To test our hypothesis that the neurological deficits of *Pum1* mutant mice resulted from an increase in Atxn1 levels due to loss of Pum1 regulation, we crossed $Pum1^{+/-}$ with $Atxn1^{+/-}$

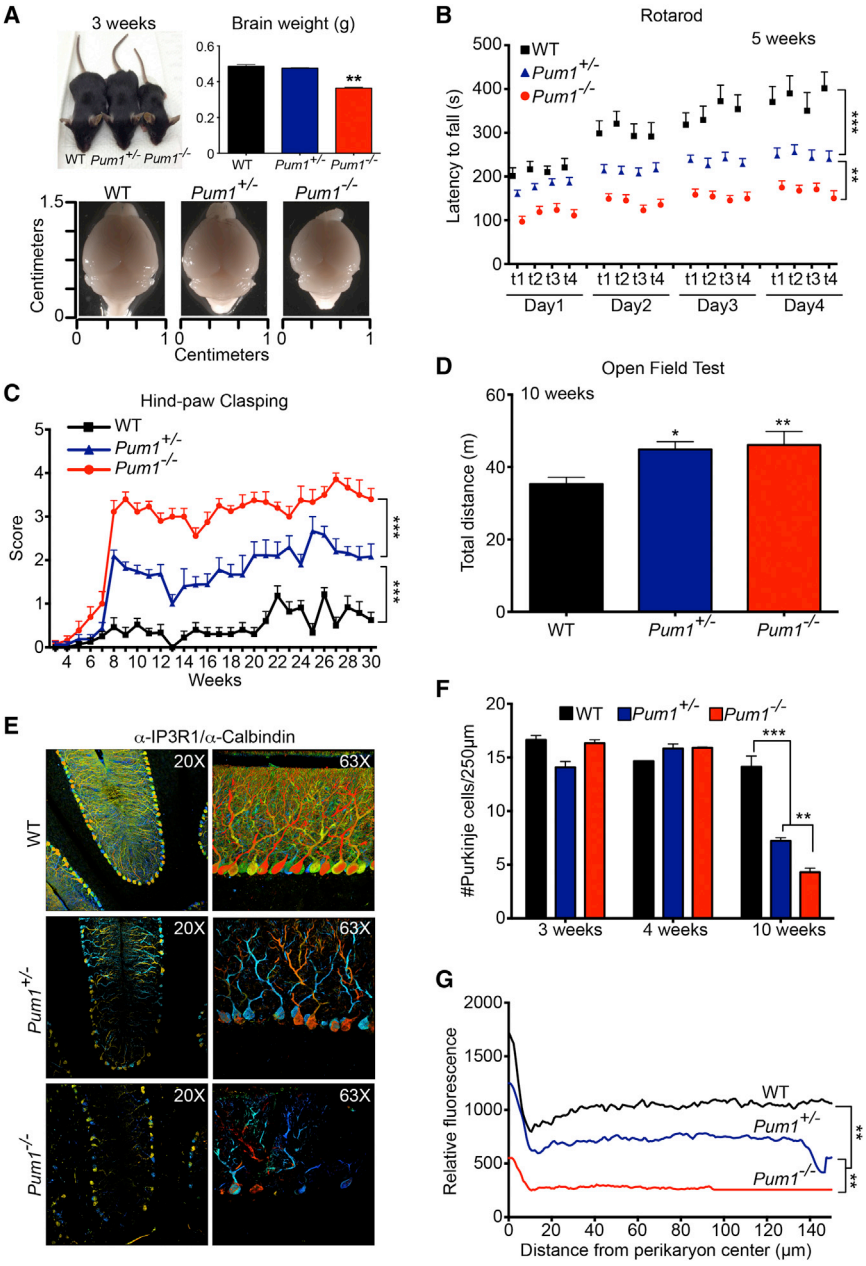

Figure 4. *Pum1* Mutant Mice Develop Progressive Motor Deficits and Cerebellar Degeneration

(A) Representative pictures of 3-week-old mice. Body size, brain weight, and brain size are reduced in *Pum1*$^{-/-}$ animals.

(B) Accelerating rotarod analysis. Mice were trained over 4 days with four trials (t) per day. The null mice were significantly different from WT from day 1; by day 2, the difference between WT and both *Pum1* null and heterozygotes was statistically significant, as was the difference between the two mutants.

(C) Hind-paw clasping analysis in mice: a higher score indicates a more severe phenotype (see Figure S4F, bottom panel for scoring details). By 6 weeks of age, the null mice were statistically different from WT; by 8 weeks, both mutant lines were statistically significantly different from WT.

(D) Open-field test measuring the total distance traveled of the *Pum1* null mice relative to WT.

(E) Representative images of immunofluorescence (IF) confocal microscopy in 3D depth-coding (see Experimental Procedures). Co-staining with α-IP3R1 and -calbindin antibodies was used to label Purkinje cells and to reveal their arborization.

(F) Purkinje cell counts at 3, 4, and 10 weeks old for all examined genotypes.

(G) IF for Calbindin and IP3R1 were quantified and averaged in selected rectangular cerebellar subsections.

All experiments were performed in WT, *Pum1*$^{+/-}$, and *Pum1*$^{-/-}$ mice. More than 12 mice per genotype were considered in (A)–(D) and 6 per genotype in (E)–(G). Data in (A), (D), and (F) represent mean ± SEM; *p < 0.05, **p < 0.01, ***p < 0.0001. See also Figure S4.

mice and characterized the offspring. We first confirmed that *Pum1* haploinsufficiency in the *Atxn1*$^{+/-}$ mice (*Pum1*$^{+/-}$;*Atxn1*$^{+/-}$) at 5 weeks completely rescued the physiological protein levels of Atxn1 (Figures 6A, S6A, and S6B). At 9 weeks, *Pum1*$^{+/-}$;*Atxn1*$^{+/-}$ mice showed no difference in body weight (Figure S5A), length, brain weight, or brain size relative to any other genotype (Figure S6C). *Atxn1* haploinsufficiency in *Pum1* mutant mice significantly mitigated the motor deficits observed in *Pum1*$^{+/-}$ animals at 5 weeks of age (Figure 6B) and completely rescued the hind-paw clasping (Figure 6C) and kyphosis, which occurs at a later age of ~25 weeks (Figure 6D). Interestingly, *Pum1*$^{+/-}$;*Atxn1*$^{+/-}$ mice still traveled farther than other genotypes and not less than *Pum1*$^{+/-}$ mice (Figure S6D). The Purkinje cell loss (Figures 6E and 6F) and arborization defects (Figure 6G) typical of 10-week-old *Pum1*$^{+/-}$ mice were rescued in *Pum1*$^{+/-}$;*Atxn1*$^{+/-}$ cerebella. This indicates that, whatever the other pathways affected by *Pum1* deficiency, the cerebellar degeneration, clasping, and kyphosis are caused primarily by the influence of Pum1 on Atxn1 levels.

Lastly, we analyzed whether *Pum1* overexpression could decrease levels of mutant (polyglutamine-expanded) Atxn1 (154Q). We used AAV8 viral injection and found that, indeed, *Atxn1*$^{154Q/+}$ mice injected with Pum1/AAV8 showed a reduction of both WT and mutant Atxn1 in the cerebellum, the region most affected in SCA1, compared to controls (*Atxn1*$^{154Q/+}$ animals injected with YFP/AAV8; Figure S6E).

DISCUSSION

Accumulation of mutant proteins in the brain has been known for some time to underlie the progression of neurodegenerative

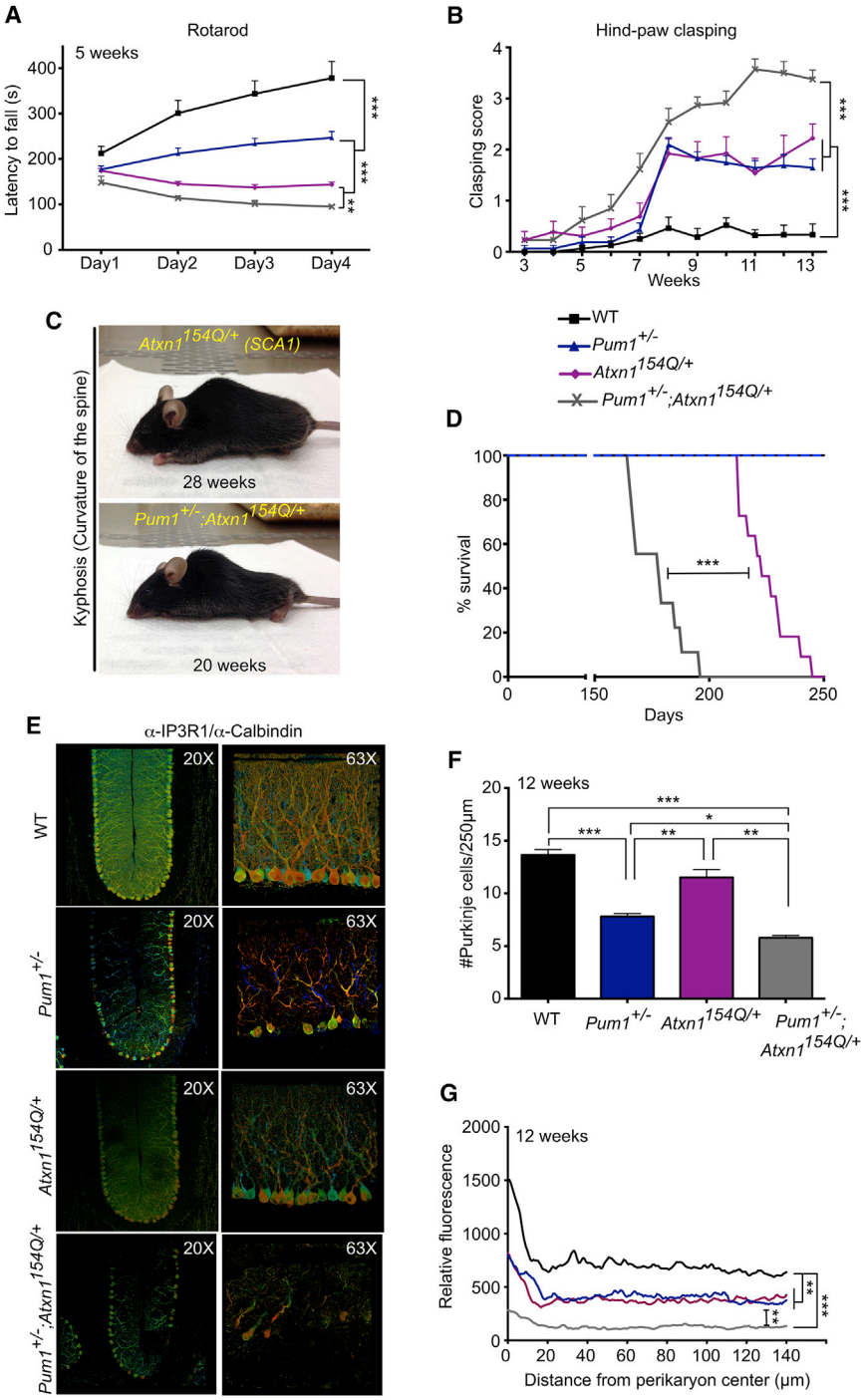

Figure 5. *Pum1* Haploinsufficiency Exacerbates SCA1 Disease Progression

(A and B) A 50% reduction of *Pum1* in *Atxn1*$^{154Q/+}$ mice aggravates (A) motor incoordination on the accelerating rotarod at 5 weeks (n = 12 per genotype) and (B) hind-paw clasping when mice are suspended by the tail (n > 12 mice per genotype). The double mutants were statistically different from WT beginning at week 6. See Experimental Procedures for details.

(C) Representative picture of SCA1 and *Pum1*$^{+/-}$;*Atxn1*$^{154Q/+}$ mice. *Pum1*$^{+/-}$;*Atxn1*$^{154Q/+}$ showed severe kyphosis (curvature of the spine) at earlier stages than their SCA1 counterparts.

(D) Haploinsufficiency of *Pum1* reduces lifespan in SCA1 background mice. p value was calculated by long-rank test; $^{**}p < 0.01$, $^{***}p < 0.0001$.

(E) Representative images of IF confocal microscopy in 3D depth-coding (see Experimental Procedures). Co-staining with α-IP3R1 and -calbindin antibodies was used to label Purkinje cells and to reveal their arborization.

(F) Purkinje cell count at 12 weeks for all examined genotypes.

(G) IF for calbindin and IP3R1 were quantified and averaged in selected rectangular cerebellar subsections.

Four mice per genotype in (E), (F), and (G) were considered. Data in (F) and (G) represent mean ± SEM; $^{*}p < 0.05$, $^{**}p < 0.01$, $^{***}p < 0.0001$. See also Figure S5.

disorders such AD, PD, HD, ALS, and the spinocerebellar ataxias. In all these diseases, the mutant proteins form insoluble aggregates (Haass and Selkoe, 2007; Klement et al., 1998; Ross and Poirier, 2004; Zoghbi and Orr, 2000). Considerable attention has been devoted to the question of whether inhibiting aggregate formation or promoting their dissolution would mitigate disease (Arrasate et al., 2004; Bowman et al., 2005, 2007). The aggregates in all these proteinopathies appear late in the disease course, however, and clearly result from processes that have been taking place for decades. Here we asked how protein levels affect the brain long before aggregates form. Specifically, we sought post-transcriptional regulatory mechanisms that regulate WT ATXN1 levels independently of the polyglutamine tract in order to determine whether reducing protein levels might delay disease progression. Our studies have unexpectedly revealed two candidate genes for neurodegenerative conditions in humans: WT (but upregulated) *ATAXIN1* and *PUMILIO1*.

We began our investigation by scanning the long 3′ UTR of ATXN1 to identify regulatory elements that could be used to modulate ATXN1 levels. We found three PUM1-binding motifs in the 3′ UTR of ATXN1, one of which is highly conserved. We used mutagenesis and RNA-Clip to show that Pum1 regulates Atxn1 levels by binding directly to the highly conserved motif in its 3′ UTR.

Pum1 is a member of a well-characterized family of RBPs, known as the PUF family, which are involved in various physiological processes (Spassov and Jurecic, 2003; Wickens et al., 2002). A typical feature of these proteins is the presence of an RNA-binding *Pumilio* homology domain (PUM-HD) that binds a

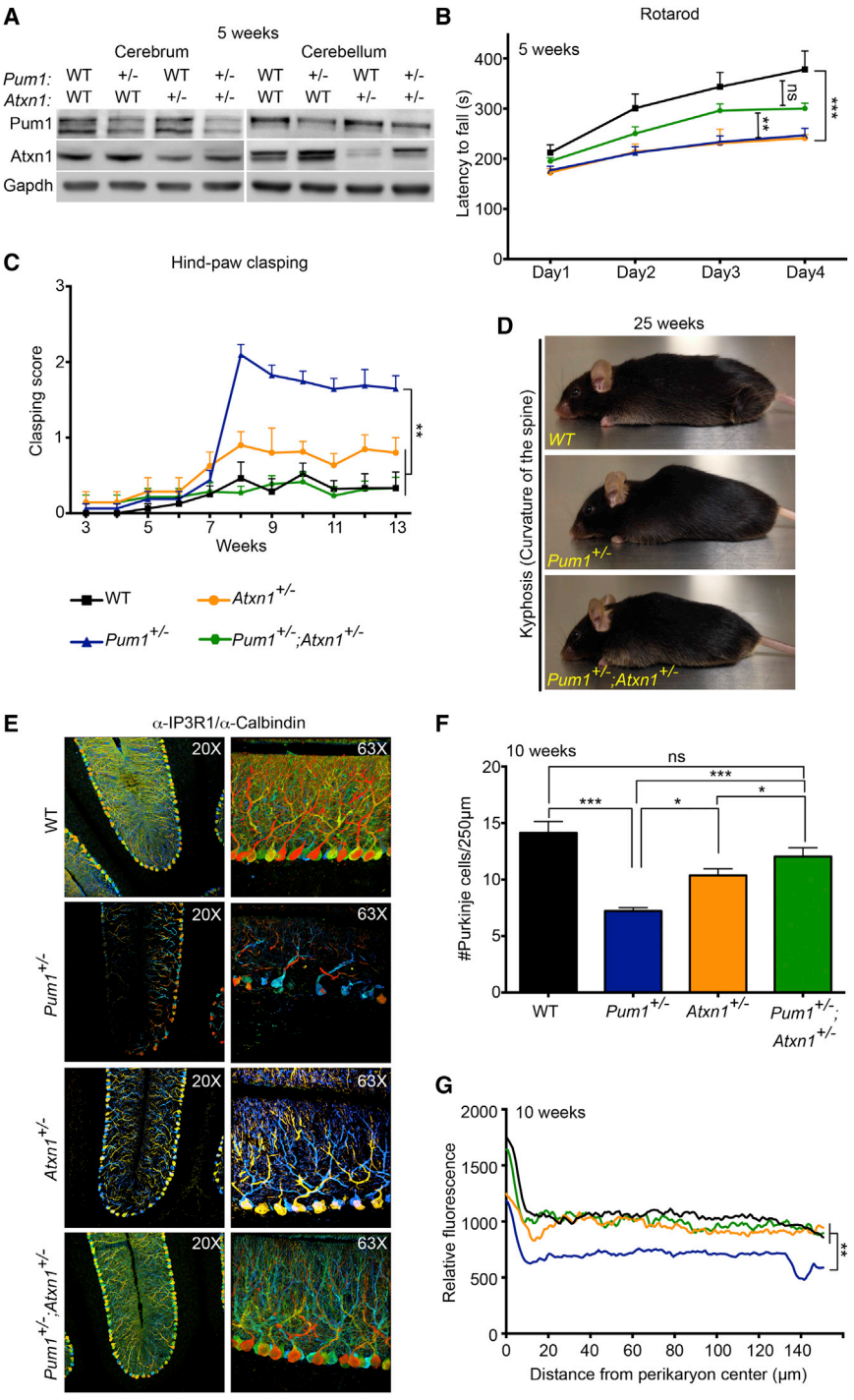

Figure 6. *Atxn1* Haploinsufficiency Rescues Motor Deficits and Cerebellar Pathology in *Pum1*$^{+/-}$ Mice

(A) Representative western blot showing that haploinsufficiency of *Pum1* restores physiological Atxn1 protein levels. All experiments were performed in triplicate in cerebra and cerebella from mice at 5 weeks of age (data represent mean ± SD). All data were normalized to Gapdh.

(B and C) *Pum1*$^{+/-}$;*Atxn1*$^{+/-}$ mice showed (B) significant improvement in motor performance on the accelerating rotarod (n = 12 per genotype), (C) reduced hind-paw clasping (n > 12 per genotype), and (D) reduced kyphosis (curvature of the spine; photo taken at 25 weeks).

(D–G) Purkinje cells loss (E and F) and loss of dendritic arborization (G) were rescued in *Pum1*$^{+/-}$;*Atxn1*$^{+/-}$ mice (n = 6 per genotype). Staining was performed with calbindin/IP3R1 in 3D deepth-coding images. Data represent mean ± SEM. See Experimental Procedures. p values was calculated by Student's t test. ns = not significant; *p < 0.05, **p < 0.01, ***p < 0.0001. See also Figure S6.

highly conserved eight-nucleotide motif (Galgano et al., 2008). PUF proteins regulate mRNA stability by several mechanisms leading to mRNA instability or translational repression (Goldstrohm et al., 2006; Suh et al., 2009). One of the most well-studied mechanisms for PUM1 activity, however, involves the miRNA machinery: PUM1 modifies the secondary structure of the 3′ UTR of its target mRNAs to allow regulation through specific miRNAs (Fabian and Sonenberg, 2012; Friend et al., 2012; Galgano et al., 2008; Kedde et al., 2010; Miles et al., 2012). It was thus surprising to find that PUM1 directly regulates *ATXN1* mRNA stability without harnessing the miRNA regulatory system.

Equally unexpected was the discovery of a role for Pum1 in the maintenance of proper brain structure and neurological function. We found *Pum1* expressed in all brain regions, but the deficits we observed in the heterozygous mice—progressive motor incoordination, hind-paw clasping, kyphosis, and Purkinje cell and dendritic degeneration—were reminiscent of the SCA1 mouse phenotype. The *Pum1* null mice phenocopied the SCA1 knockin mice but developed even more severe Purkinje cell pathology, showing significant neuronal loss after only 2 months. We believe this is explained at least in part by constitutive ~50% increase in WT Atxn1 in contrast with the gradual nature of the accumulation of polyglutamine-expanded proteins. Even in the SCA1 knockin mice, the mutant protein takes time to accumulate to levels that produce symptoms. In the *Pum1* mutants, however, the levels of Atxn1 are elevated from the very beginning of life.

The dramatic exacerbation of disease progression in SCA1 knockin mice lacking a copy of *Pum1* indicates a genetic interaction between *Pumilio1* and *Ataxin1*, but the precocity of disease symptoms in the double mutants could conceivably

arise through either of two mechanisms: the loss of one copy of Pum1 directly increasing levels of mutant Atxn1, or an additive effect ascribable to the combination of two severe mutations (loss of *Pum1* and the CAG expansion in *Atxn1*). Our results argue for the former possibility. First, the defects observed in *Pum1* mutant mice were largely corrected by reducing *Atxn1* levels. Second, the *Pum1*$^{+/-}$;*Atxn1*$^{+/-}$ mice were healthier than either *Pum1*$^{+/-}$ or *Atxn1*$^{+/-}$ mice. Third, we found that viral overexpression of Pum1 in the mouse brain reduced both the WT and expanded [154Q] forms of the Atxn1 protein (Figure S6E). These three facts support the notion that the neurological deficits exhibited by the *Pum1* mutant mice are caused primarily by a rise in WT Atxn1 levels, even though other Pum1 targets are undoubtedly affected as well. Without knowing the full set of Pum1 targets, we cannot rule out all other pathways, but we were able to evaluate levels of two well-studied PUM1 targets, E2F3 and p27, in *Pum1*$^{+/-}$as well as *Pum1*$^{+/-}$;*Atxn1*$^{+/-}$ mice. We did not find any significant change in the levels of these two proteins in the cerebella of either *Pum1*$^{+/-}$ *or Pum1*$^{+/-}$;*Atxn1*$^{+/-}$ mice compared to other genotypes (data not shown).

It is well established that the severity of neurodegeneration in SCA1 correlates with the levels of expanded (or even WT) ATXN1 and that decreasing ATXN1 accumulation can reverse the disease phenotypes in SCA1 models (Fernandez-Funez et al., 2000; Park et al., 2013). It has been only relatively recently, however, that we have understood that in some neurodegenerative diseases, such as AD and PD, too much of the WT protein can produce the same phenotype as the mutant protein (Chartier-Harlin et al., 2004; Ibáñez et al., 2004; Rovelet-Lecrux et al., 2006; Rumble et al., 1989; Singleton et al., 2003). Our first study of transgenic mice overexpressing WT human ATXN1[30Q] under the control of a Purkinje-cell-specific promoter (*Pcp2-Atxn1-(CAG)30Q*) failed to reveal cerebellar pathology or ataxia (Burright et al., 1995), but our later work monitoring the mice throughout their lifespans revealed that *Pcp2-Atxn1-(CAG)30Q* mice develop mild Purkinje cell degeneration in later life (Fernandez-Funez et al., 2000). This suggested that only dramatic overexpression of WT ATXN1 would be neurotoxic, but the artificiality of the transgenic model—ATXN1 cDNA was massively and postnatally expressed only in cerebellar Purkinje cells and without the 3′ UTR—limited its relevance for human patients. Here we introduce the evidence that a moderate (30%–60%) increase in the levels of endogenous WT Atxn1, expressed in the correct temporal and spatial pattern throughout the brain and preserving all its regulatory elements, is deleterious to neuronal function.

Atxn1 is expressed throughout the brain (Figure S2A) from very early embryonic stages (Banfi et al., 1994, 1996; Servadio et al., 1995). The present study suggests that mutations in *PUM1* or copy-number changes in *ATXN1* could cause cerebellar neurodegeneration in humans by increasing the levels of ATXN1 throughout development. Variations in *PUM1* or other factors that govern ATXN1 levels could also underlie the individual differences in SCA1 onset for the same CAG repeat length.

In conclusion, we propose that identifying molecules capable of regulating ATXN1 levels provides insight into factors that contribute to cerebellar degeneration. We further propose that studying factors that regulate the RNA stability of proteins such as APP, TAU, or a-SYN might uncover candidate genes as well as binding sites whose mutation could lead to AD or PD—two diseases for which our understanding of molecular genetic causes is still very limited. For these and the ever-lengthening list of neurodegenerative conditions that do not fit Mendelian categories, it may prove most fruitful to search for factors that elevate the levels of key disease-driving proteins.

EXPERIMENTAL PROCEDURES

Bioinformatic Analysis

The *ATXN1*-3′ UTR was downloaded from UTRdb (Grillo et al., 2010). The ATXN1 3′ UTR was scanned against CoMeTa (Gennarino et al., 2012), HOCTARdb (Gennarino et al., 2011), and TargetScan (Friedman et al., 2009) to identify all putative miRNAs regulating ATXN1. The secondary structure of *ATXN1*-3′ UTR was calculated with the Vienna RNAfold (Gruber et al., 2008) package by using default parameters in a Minimum Free energy "MFE" (Zuker and Stiegler, 1981) and Boltzmann ensemble "Centroid" (Hofacker and Stadler, 2006). *ATXN1*-3′ UTR was scanned against all known RBP motifs downloaded from the database of RBP specificities (RBPDB) (Cook et al., 2011).

Cell Culture and Transfection

The Human embryonic kidney immortalized 293 cells (HEK293T) were grown in DMEM (Invitrogen), supplemented with 10% of heat-inactivated fetal bovine serum (FBS) and penicillin/streptomycin. All cells were incubated at 37°C in a humidified chamber supplemented with 5% CO_2. Transfection of HEK293T cells was performed using jetPRIME Transfection Reagent (Polyplus transfection) according to the manufacturer's protocol. Cells were transfected with 50 pmol of either miRIDIAN Dharmacon microRNA Mimics (miR-101a or negative control cel-miR-67) or Ambion small interfering RNA (*siAGO2*, *siPUM1*, or scramble-*siRNA* control). For overexpression studies, the full cDNA of *PUM1* (4,635 nt) was amplified by Platinum Taq DNA Polymerase High Fidelity (Invitrogen) and cloned into a mammalian expression vector termed pcDNA3.1(+) (Invitrogen). Cells were transfected with 0.5 μg of either pcDNA3.1(+)-PUM1 or control pcDNA3.1(+).

RNA Extraction and Quantitative Real-Time PCR

HEK293T cells were seeded in 6-well plates before transfection. After 48 hr, cells were collected and processed for RNA extraction. Total RNA was obtained using the miRNeasy kit (Quiagen) according to the manufacturer's instructions. RNA extraction from mouse cerebrum or cerebellum was extracted from 75 mg of tissue. RNA was quantified using the NanoDrop 1000 (Thermo Fisher). Quality of RNA was assessed by gel electrophoresis. cDNA was synthesized using Quantitect Reverse Transcription kit (Quiagen) starting from 1 μg of DNase-treated RNA. qRT-PCR experiments were performed using the CFX96 Touch Real-Time PCR Detection System (Bio-Rad Laboratories) with PerfeCta SYBR Green FastMix, ROX (Quanta Biosciences). Real-time PCR results were analyzed using the comparative Ct method normalized against the housekeeping gene *GAPDH* (Vandesompele et al., 2002). The range of expression levels was determined by calculating the standard deviation of the ΔCt (Pfaffl, 2001).

Luciferase Assay

The full-length 3′ UTR of human *ATXN1* mRNA was subcloned into psiCHECK-2 vector (Promega) by XbaI and NheI restriction enzymes (Lee et al., 2008). The partial 3′ UTR, containing binding sites 1 (582–782), 2 (2712–2912), and 3 (5175–5375), was amplified by PCR and cloned into psiCHECK-2 vector (Promega). Mutagenesis reactions were performed using the QuikChange XL Site-Directed Mutagenesis kit (Stratagene). Primers for mutagenesis analysis were automatically designed by QuickChange software (Stratagene). HEK293T cells in 24-well plates were transfected with 30 ng of psiCHECK-2 construct plus the following: 50 pmol of si*PUM1* or control scramble-siRNA and 0.5 μg of pcDNA3.1(+)-*PUM1* or control pcDNA3.1(+)

using Lipofectamine 2000 (Invitrogen). After 24 hr, luciferase activity was measured using the Dual Luciferase Reporter Assay System (Promega) according to the manufacturer's instructions.

Western Blot

HEK293T cells were seeded in 6-well plates before transfection. After 72 hr, cells were processed for protein extraction. For mouse tissues, the entire cerebrum and cerebellum were processed for protein extraction. Both pellet and tissues were lysed with RIPA buffer (25 mM Tris-HCL, pH 7.6, 150 mM NaCl, 1% NP-40, 1% sodium deoxycholate, 0.1% SDS, and complete protease inhibitor cocktail [Roche]), then placed for 15 min on ice followed by centrifugation at 13,000 rpm at 4°C for 15 min. Proteins were quantified by Pierce BCA Protein Assay Kit (Thermo Scientific) and resolved by high-resolution Bolt 4%–12% Bis-Tris Plus Gel (Life Technologies) according to the manufacturer's instruction.

RNA-CLIP

Brains from WT or *Pum1* knockout mice were dissected out, and cerebella were separated from the rest of the brains. After separation, the tissue was triturated in 8 ml of ice-cold HBSS until cells were evenly dissociated with no visible chunks. The cell suspension was layered on a chilled 10 cm sterile tissue culture plate and exposed to 150 mJ/cm^2 UVC (Stratagene, model UV Stratalinker 2400) on ice. After one exposure, the cell suspension was gently swirled and exposed again to UVC at 100 mJ/cm^2. The cell suspension was pelleted for individual immunoprecipitation (IP). Cells were lysed in lysis buffer (50 mMTris-HCl, pH 7.4, 100 mMNaCl, 1% NP-40, 0.1% SDS, 0.5% sodium deoxycholate, 80 U/ml RNase OUT [Invitrogen] with protease inhibitor [Roche]). Soluble fractions were pre-cleared with protein A-sepharose beads, rabbit control IgG (Sigma), 0.05% BSA, and 0.2 μg/ml yeast tRNA (Invitrogen). Pre-cleared lysates were incubated with control IgG or Pum1 (5 μg) (Bethyl Laboratories, see Antibodies) together with protein A-sepharose beads and incubated overnight at 4°C with gentle rotation. Next day, beads were washed five times with lysis buffer. Beads were treated using 20 units of RNase-free DNase (Roche) for 15 min at room temperature, followed by 50 μg proteinase K (Roche) treatment for 30 min at 37°C. Immunoprecipated RNA was isolated using miRNeasy kit (Quiagen), and RT-PCR was performed using primers designed to amplify *Atxn1* cDNA regions upstream and downstream of the predicted *Pum1*-binding site (see Primers). Isolated RNA from a fraction (10%) of pre-cleared lysate was used as input.

RNA Stability

Total RNA from HEK293T cells, RNA quality, cDNA synthesized, and qRT-PCR experiments were obtained as described above in RNA Extraction and Quantitative Real-Time PCR. HEK293T cells were seeded in 24-well plates before transfection for both experiments (Figures 3E and 3F). For Figure 3E, the partial 3′ UTR containing the PUM1 WT or Mut binding sites 3 (5175–5375) were the same as used for the luciferase assay (see Luciferase Assay section). HEK293T cells were transfected with 30 ng of psiCHECK-2 vectors (Promega) containing *ATXN1*-3′ UTR WT or Mut binding sites using Lipofectamine 2000 (Invitrogen). After 36 hr, cells were treated with 5,6-dichloro-1-β-D-ribofuranosylbenzimidazole (DRB) at the final concentration of 20 μg/ml, and total RNA for qRT-PCR analysis was collected at different time points. *Firefly* data were normalized to the respective *Renilla*. For Figure 3F, HEK293T cells were transfected with Ambion siRNA for *PUM1* (si*PUM1*) or Scramble (siScramble) at the final concentration of 40 nM. After 48 hr, cells were collected, and the total RNA was processed for qRT-PCR. All data were normalized to *GAPDH*. The housekeeping gene *GAPDH* was used to compare all the qRT-PCR values. All western blot experiments were performed as described in the Western Blot section.

SUPPLEMENTAL INFORMATION

Supplemental Information includes Extended Experimental Procedures and six figures and can be found with this article online at http://dx.doi.org/10.1016/j.cell.2015.02.012.

AUTHOR CONTRIBUTIONS

V.A.G. and H.Y.Z. conceived the study, designed experiments, analyzed and interpreted data, and wrote the manuscript. V.A.G. performed molecular and behavioral tests. R.K.S., J.J.W., A.D.M., K.H., J.-Y.K., P.J.-N., A.D.R., and L.S.S. contributed to molecular work. H.K. performed bioinformatic analyses. T.A.C., H.T.O., and R.V.S. contributed to interpreting data.

ACKNOWLEDGMENTS

We thank Dr. Haifan Lin (Yale Stem Cell Center and Department of Cell Biology, Yale University School of Medicine) for sharing the *Pum1* mutant mice; A. McCall for helpful suggestions on analysis; X. Liu for genotyping; C. Spencer for behavioral training; C. Ljungberg for ISH analysis; D. Yu for confocal microscopy training; and members of the H.Y.Z. laboratory for helpful discussions. We also thank A. Ballabio, T. Klisch, S. Yamamoto, M. Rousseaux, M. Sardiello, C. Schaaf, C. Alcott, and V. Brandt for helpful suggestions and critical reading of the manuscript. This research was supported by R01NS027699-26 (to H.Y.Z.) and the RNA In Situ Hybridization, Confocal and Mouse Behavioral Cores at the BCM Intellectual and Developmental Disabilities Research Center (IDDRC; NIH/NICHHDP30-HD024064) and 1R01NS089664-01 (to R.V.S.). The content is solely the responsibility of the authors and does not necessarily represent the official views of the Eunice Kennedy Shriver National Institute of Child Health & Human Development or the National Institutes of Health.

Received: July 22, 2014
Revised: December 1, 2014
Accepted: January 30, 2015
Published: March 12, 2015

REFERENCES

Arrasate, M., Mitra, S., Schweitzer, E.S., Segal, M.R., and Finkbeiner, S. (2004). Inclusion body formation reduces levels of mutant huntingtin and the risk of neuronal death. Nature *431*, 805–810.

Banfi, S., Servadio, A., Chung, M.Y., Kwiatkowski, T.J., Jr., McCall, A.E., Duvick, L.A., Shen, Y., Roth, E.J., Orr, H.T., and Zoghbi, H.Y. (1994). Identification and characterization of the gene causing type 1 spinocerebellar ataxia. Nat. Genet. *7*, 513–520.

Banfi, S., Servadio, A., Chung, M., Capozzoli, F., Duvick, L.A., Elde, R., Zoghbi, H.Y., and Orr, H.T. (1996). Cloning and developmental expression analysis of the murine homolog of the spinocerebellar ataxia type 1 gene (Sca1). Hum. Mol. Genet. *5*, 33–40.

Bartel, D.P. (2009). MicroRNAs: target recognition and regulatory functions. Cell *136*, 215–233.

Bhattacharyya, S.N., Habermacher, R., Martine, U., Closs, E.I., and Filipowicz, W. (2006). Relief of microRNA-mediated translational repression in human cells subjected to stress. Cell *125*, 1111–1124.

Bowman, A.B., Yoo, S.Y., Dantuma, N.P., and Zoghbi, H.Y. (2005). Neuronal dysfunction in a polyglutamine disease model occurs in the absence of ubiquitin-proteasome system impairment and inversely correlates with the degree of nuclear inclusion formation. Hum. Mol. Genet. *14*, 679–691.

Bowman, A.B., Lam, Y.C., Jafar-Nejad, P., Chen, H.K., Richman, R., Samaco, R.C., Fryer, J.D., Kahle, J.J., Orr, H.T., and Zoghbi, H.Y. (2007). Duplication of Atxn1l suppresses SCA1 neuropathology by decreasing incorporation of polyglutamine-expanded ataxin-1 into native complexes. Nat. Genet. *39*, 373–379.

Burright, E.N., Clark, H.B., Servadio, A., Matilla, T., Feddersen, R.M., Yunis, W.S., Duvick, L.A., Zoghbi, H.Y., and Orr, H.T. (1995). SCA1 transgenic mice: a model for neurodegeneration caused by an expanded CAG trinucleotide repeat. Cell *82*, 937–948.

Chartier-Harlin, M.C., Kachergus, J., Roumier, C., Mouroux, V., Douay, X., Lincoln, S., Levecque, C., Larvor, L., Andrieux, J., Hulihan, M., et al. (2004). Alpha-synuclein locus duplication as a cause of familial Parkinson's disease. Lancet *364*, 1167–1169.

Chen, D., Zheng, W., Lin, A., Uyhazi, K., Zhao, H., and Lin, H. (2012). Pumilio 1 suppresses multiple activators of p53 to safeguard spermatogenesis. Curr. Biol. *22*, 420–425.

Cook, K.B., Kazan, H., Zuberi, K., Morris, Q., and Hughes, T.R. (2011). RBPDB: a database of RNA-binding specificities. Nucleic Acids Res. *39* (Database issue), D301–D308.

Cummings, C.J., Reinstein, E., Sun, Y., Antalffy, B., Jiang, Y., Ciechanover, A., Orr, H.T., Beaudet, A.L., and Zoghbi, H.Y. (1999). Mutation of the E6-AP ubiquitin ligase reduces nuclear inclusion frequency while accelerating polyglutamine-induced pathology in SCA1 mice. Neuron *24*, 879–892.

Fabian, M.R., and Sonenberg, N. (2012). The mechanics of miRNA-mediated gene silencing: a look under the hood of miRISC. Nat. Struct. Mol. Biol. *19*, 586–593.

Fernandez-Funez, P., Nino-Rosales, M.L., de Gouyon, B., She, W.C., Luchak, J.M., Martinez, P., Turiegano, E., Benito, J., Capovilla, M., Skinner, P.J., et al. (2000). Identification of genes that modify ataxin-1-induced neurodegeneration. Nature *408*, 101–106.

Friedman, R.C., Farh, K.K., Burge, C.B., and Bartel, D.P. (2009). Most mammalian mRNAs are conserved targets of microRNAs. Genome Res. *19*, 92–105.

Friend, K., Campbell, Z.T., Cooke, A., Kroll-Conner, P., Wickens, M.P., and Kimble, J. (2012). A conserved PUF-Ago-eEF1A complex attenuates translation elongation. Nat. Struct. Mol. Biol. *19*, 176–183.

Galgano, A., Forrer, M., Jaskiewicz, L., Kanitz, A., Zavolan, M., and Gerber, A.P. (2008). Comparative analysis of mRNA targets for human PUF-family proteins suggests extensive interaction with the miRNA regulatory system. PLoS ONE *3*, e3164.

Gennarino, V.A., Sardiello, M., Mutarelli, M., Dharmalingam, G., Maselli, V., Lago, G., and Banfi, S. (2011). HOCTAR database: a unique resource for microRNA target prediction. Gene *480*, 51–58.

Gennarino, V.A., D'Angelo, G., Dharmalingam, G., Fernandez, S., Russolillo, G., Sanges, R., Mutarelli, M., Belcastro, V., Ballabio, A., Verde, P., et al. (2012). Identification of microRNA-regulated gene networks by expression analysis of target genes. Genome Res. *22*, 1163–1172.

Glorian, V., Maillot, G., Polès, S., Iacovoni, J.S., Favre, G., and Vagner, S. (2011). HuR-dependent loading of miRNA RISC to the mRNA encoding the Ras-related small GTPase RhoB controls its translation during UV-induced apoptosis. Cell Death Differ. *18*, 1692–1701.

Goldstrohm, A.C., Hook, B.A., Seay, D.J., and Wickens, M. (2006). PUF proteins bind Pop2p to regulate messenger RNAs. Nat. Struct. Mol. Biol. *13*, 533–539.

Grillo, G., Turi, A., Licciulli, F., Mignone, F., Liuni, S., Banfi, S., Gennarino, V.A., Horner, D.S., Pavesi, G., Picardi, E., and Pesole, G. (2010). UTRdb and UTRsite (RELEASE 2010): a collection of sequences and regulatory motifs of the untranslated regions of eukaryotic mRNAs. Nucleic Acids Res. *38* (Database issue), D75–D80.

Gruber, A.R., Lorenz, R., Bernhart, S.H., Neuböck, R., and Hofacker, I.L. (2008). The Vienna RNA websuite. Nucleic Acids Res. *36* (Web Server issue), W70–W74.

Haass, C., and Selkoe, D.J. (2007). Soluble protein oligomers in neurodegeneration: lessons from the Alzheimer's amyloid beta-peptide. Nat. Rev. Mol. Cell Biol. *8*, 101–112.

Hofacker, I.L., and Stadler, P.F. (2006). Memory efficient folding algorithms for circular RNA secondary structures. Bioinformatics *22*, 1172–1176.

Ibáñez, P., Bonnet, A.M., Débarges, B., Lohmann, E., Tison, F., Pollak, P., Agid, Y., Dürr, A., and Brice, A. (2004). Causal relation between alpha-synuclein gene duplication and familial Parkinson's disease. Lancet *364*, 1169–1171.

Kedde, M., van Kouwenhove, M., Zwart, W., Oude Vrielink, J.A., Elkon, R., and Agami, R. (2010). A Pumilio-induced RNA structure switch in p27-3′ UTR controls miR-221 and miR-222 accessibility. Nat. Cell Biol. *12*, 1014–1020.

Kim, H.H., Kuwano, Y., Srikantan, S., Lee, E.K., Martindale, J.L., and Gorospe, M. (2009). HuR recruits let-7/RISC to repress c-Myc expression. Genes Dev. *23*, 1743–1748.

Klement, I.A., Skinner, P.J., Kaytor, M.D., Yi, H., Hersch, S.M., Clark, H.B., Zoghbi, H.Y., and Orr, H.T. (1998). Ataxin-1 nuclear localization and aggregation: role in polyglutamine-induced disease in SCA1 transgenic mice. Cell *95*, 41–53.

Kundu, P., Fabian, M.R., Sonenberg, N., Bhattacharyya, S.N., and Filipowicz, W. (2012). HuR protein attenuates miRNA-mediated repression by promoting miRISC dissociation from the target RNA. Nucleic Acids Res. *40*, 5088–5100.

Lee, Y., Samaco, R.C., Gatchel, J.R., Thaller, C., Orr, H.T., and Zoghbi, H.Y. (2008). miR-19, miR-101 and miR-130 co-regulate ATXN1 levels to potentially modulate SCA1 pathogenesis. Nat. Neurosci. *11*, 1137–1139.

Leeb, M., Dietmann, S., Paramor, M., Niwa, H., and Smith, A. (2014). Genetic exploration of the exit from self-renewal using haploid embryonic stem cells. Cell Stem Cell *14*, 385–393.

Lukong, K.E., Chang, K.W., Khandjian, E.W., and Richard, S. (2008). RNA-binding proteins in human genetic disease. Trends Genet. *24*, 416–425.

Martin, I., Kim, J.W., Lee, B.D., Kang, H.C., Xu, J.C., Jia, H., Stankowski, J., Kim, M.S., Zhong, J., Kumar, M., et al. (2014). Ribosomal protein s15 phosphorylation mediates LRRK2 neurodegeneration in Parkinson's disease. Cell *157*, 472–485.

Miles, W.O., Tschöp, K., Herr, A., Ji, J.Y., and Dyson, N.J. (2012). Pumilio facilitates miRNA regulation of the E2F3 oncogene. Genes Dev. *26*, 356–368.

Orr, H.T., Chung, M.Y., Banfi, S., Kwiatkowski, T.J., Jr., Servadio, A., Beaudet, A.L., McCall, A.E., Duvick, L.A., Ranum, L.P., and Zoghbi, H.Y. (1993). Expansion of an unstable trinucleotide CAG repeat in spinocerebellar ataxia type 1. Nat. Genet. *4*, 221–226.

Park, J., Al-Ramahi, I., Tan, Q., Mollema, N., Diaz-Garcia, J.R., Gallego-Flores, T., Lu, H.C., Lagalwar, S., Duvick, L., Kang, H., et al. (2013). RAS-MAPK-MSK1 pathway modulates ataxin 1 protein levels and toxicity in SCA1. Nature *498*, 325–331.

Pfaffl, M.W. (2001). A new mathematical model for relative quantification in real-time RT-PCR. Nucleic Acids Res. *29*, e45.

Ross, C.A., and Poirier, M.A. (2004). Protein aggregation and neurodegenerative disease. Nat. Med. Suppl. *10*, S10–S17.

Rovelet-Lecrux, A., Hannequin, D., Raux, G., Le Meur, N., Laquerrière, A., Vital, A., Dumanchin, C., Feuillette, S., Brice, A., Vercelletto, M., et al. (2006). APP locus duplication causes autosomal dominant early-onset Alzheimer disease with cerebral amyloid angiopathy. Nat. Genet. *38*, 24–26.

Rumble, B., Retallack, R., Hilbich, C., Simms, G., Multhaup, G., Martins, R., Hockey, A., Montgomery, P., Beyreuther, K., and Masters, C.L. (1989). Amyloid A4 protein and its precursor in Down's syndrome and Alzheimer's disease. N. Engl. J. Med. *320*, 1446–1452.

Servadio, A., Koshy, B., Armstrong, D., Antalffy, B., Orr, H.T., and Zoghbi, H.Y. (1995). Expression analysis of the ataxin-1 protein in tissues from normal and spinocerebellar ataxia type 1 individuals. Nat. Genet. *10*, 94–98.

Singleton, A.B., Farrer, M., Johnson, J., Singleton, A., Hague, S., Kachergus, J., Hulihan, M., Peuralinna, T., Dutra, A., Nussbaum, R., et al. (2003). alpha-Synuclein locus triplication causes Parkinson's disease. Science *302*, 841.

Soto, C. (2003). Unfolding the role of protein misfolding in neurodegenerative diseases. Nat. Rev. Neurosci. *4*, 49–60.

Spassov, D.S., and Jurecic, R. (2003). The PUF family of RNA-binding proteins: does evolutionarily conserved structure equal conserved function? IUBMB Life *55*, 359–366.

Suh, N., Crittenden, S.L., Goldstrohm, A., Hook, B., Thompson, B., Wickens, M., and Kimble, J. (2009). FBF and its dual control of gld-1 expression in the Caenorhabditis elegans germline. Genetics *181*, 1249–1260.

Vandesompele, J., De Preter, K., Pattyn, F., Poppe, B., Van Roy, N., De Paepe, A., and Speleman, F. (2002). Accurate normalization of real-time quantitative RT-PCR data by geometric averaging of multiple internal control genes. Genome Biol. *3*, H0034.

Wan, Y., Qu, K., Zhang, Q.C., Flynn, R.A., Manor, O., Ouyang, Z., Zhang, J., Spitale, R.C., Snyder, M.P., Segal, E., and Chang, H.Y. (2014). Landscape and variation of RNA secondary structure across the human transcriptome. Nature *505*, 706–709.

Wang, X., McLachlan, J., Zamore, P.D., and Hall, T.M. (2002). Modular recognition of RNA by a human pumilio-homology domain. Cell *110*, 501–512.

Watase, K., Weeber, E.J., Xu, B., Antalffy, B., Yuva-Paylor, L., Hashimoto, K., Kano, M., Atkinson, R., Sun, Y., Armstrong, D.L., et al. (2002). A long CAG repeat in the mouse Sca1 locus replicates SCA1 features and reveals the impact of protein solubility on selective neurodegeneration. Neuron *34*, 905–919.

Wickens, M., Bernstein, D.S., Kimble, J., and Parker, R. (2002). A PUF family portrait: 3'UTR regulation as a way of life. Trends Genet. *18*, 150–157.

Zoghbi, H.Y., and Orr, H.T. (2000). Glutamine repeats and neurodegeneration. Annu. Rev. Neurosci. *23*, 217–247.

Zoghbi, H.Y., and Orr, H.T. (2009). Pathogenic mechanisms of a polyglutamine-mediated neurodegenerative disease, spinocerebellar ataxia type 1. J. Biol. Chem. *284*, 7425–7429.

Zuker, M., and Stiegler, P. (1981). Optimal computer folding of large RNA sequences using thermodynamics and auxiliary information. Nucleic Acids Res. *9*, 133–148.